JOURNAL OF PRODUCTION ENGINEERING VOL. 29, NO. 1 (2026)
DOI: 10.24867/JPE-2026-01-021

Original research article

Journal of
Production Engineering

https://jpe.ftn.uns.ac.rs/index.php/jpe
ISSN: 1821-4932 (print), ISSN: 2956-2252 (online)

Dynamic simulation framework for single-tooth crack detection in spur gearboxes: modal analysis and vibration indicator sensitivity

Mohsen Meshkini 0000-0002-1958-9631, ***Ali Selk Ghafari*** * 0000-0003-0643-6588

Sharif University of Technology International Campus, kish Island, Iran.

ABSTRACT

This study introduces an efficient dynamic simulation framework for a single-stage spur gearbox with an induced single-tooth crack, aimed at evaluating vibration-based health indicators for early crack propagation detection. Building upon the conventional lumped parameter approach, the model incorporates an advanced continuous mesh stiffness function, capturing crack-induced variations in stiffness and damping while integrating torsional degrees of freedom. The dynamic analysis, focusing on y-axis motion and neglecting frictional effects, employs a six-degree-of-freedom model to compute natural frequencies, lateral mode shapes, receptance and phase responses, mobility and accelerance characteristics, and Nyquist plots to comprehensively characterize system dynamics. Relative damping ratios are determined using the peak picking method, while the Ibrahim Time Domain method yields time-domain responses and refined natural frequencies. Health indicator analysis demonstrates that Root Mean Square (RMS) values, extracted from residual signal segments corresponding to the first three meshing cycles, exhibit superior sensitivity to early crack propagation compared to Kurtosis. Discrete Wavelet Transform (DWT) preprocessing significantly enhances RMS sensitivity, with an optimal decomposition level identified; exceeding this level results in diminished monotonicity and sensitivity. The methodology proves robust under noisy conditions, though elevated noise levels reduce both sensitivity and the optimal DWT level. Validation across diverse gearbox sizes and input shaft frequencies confirms the approach's generalizability. This framework establishes a highly effective, robust strategy for vibration-based condition monitoring, offering substantial potential for early fault detection and strategic maintenance planning in critical industrial gear systems.

ARTICLE INFO

Received: 31 January 2026
Revised: 28 April 2026
Accepted: 18 May 2026

KEYWORDS:
Spur Gearbox;
Tooth Crack Propagation;
Vibration-Based Monitoring;
Discrete Wavelet Transform (DWT);
Modal Analysis.

**Corresponding author's.e-mail: a_selkghafari@sharif.edu*

1. INTRODUCTION

Gearboxes are critical components in mechanical systems, enabling efficient power transmission in applications ranging from automotive to wind energy and industrial rotating machinery. Their intricate kinematic and dynamic interactions make them perfect for compact and high-torque applications [1]. However, any mechanical faults, such as tooth cracks, can lead to operational fatigue, reduced efficiency, and safety hazards [1,2]. Simulation-based approaches allow researchers to study fault dynamics under controlled conditions, and reduce the high costs and time associated with physical experiments [3]. Vibration-based condition monitoring has become essential for gearbox diagnostics, leveraging experimental and field measurements to develop robust fault detection methodologies [4]. Vibration analysis techniques are categorized into time-domain, frequency-domain, time-frequency, and artificial intelligence-based methods. Statistical indicators, such as spectral kurtosis proposed by Brown et al. [5], enable fault detection by identifying deviations in vibration signal characteristics. Modal analysis is pivotal for understanding gearbox dynamics, employing techniques such as Experimental Modal Analysis (EMA), Operational Modal Analysis (OMA), and Order-Based Modal Analysis (OBMA). EMA, utilizing

Published by the University of Novi Sad, Faculty of Technical Sciences, Novi Sad, Serbia.

impact or shaker tests, estimates natural frequencies, modal damping, and mode shapes [6], but faces challenges including repeated testing, discrepancies between lab and operational conditions, and structural loading from shakers [7]. Mbarek et al. [8] applied EMA to planetary gears, validating results against lumped parameter and finite element models, while Hammami [9] developed a rotational lumped-parameter model for torsional natural frequencies. Tatar et al. [10] proposed a translational-rotational coupled model for planetary gear sets. OMA, an output-only method, characterizes modal properties under operational conditions, suitable for rotating machinery [11, 12]. Manzato et al. [13], Gade et al. [14] and van Vondelen et al. [15] introduced automated damping estimation for wind turbine gearboxes. OBMA extracts modal properties during run-up or run-down tests, as shown by Hammami et al. [16]. Xia et al. [17] proposed methods to remove variable-speed harmonic orders, and Zhang et al. [18] utilized the Vold-Kalman Filter for robust modal parameter estimation in noisy conditions. Comparative studies by Zhang et al. [19], and Mbarek et al. [20] highlight differences in natural frequency estimation, with OMA and OBMA often exhibiting higher damping due to operational conditions. Advanced dynamic models have enhanced the understanding of gearbox fault dynamics. Zhou et al. [21] and Omar et al. [22] investigated tooth crack effects on spur gearbox vibrations using lumped parameter models, while others emphasized modal parameters, gear mesh stiffness, and boundary conditions [23-28]. Simulations incorporating torsional and lateral vibrations, friction, and crack effects provide comprehensive insights [21, 29]. Recent planetary gear studies have applied OBMA to characterize dynamics in wind turbine gearboxes and precision test rigs [30]. Despite these advancements, early detection of crack propagation under varying operational conditions and noise remains a challenge, necessitating sensitive and robust health indicators. This study addresses this gap by developing a dynamic model of a single-stage spur gearbox with a single-tooth crack to evaluate vibration-based health indicators, including root mean square (RMS), Kurtosis, and the discrete wavelet transform (DWT) technique. Extending the work of Omar et al. [22] with an enhanced continuous mesh stiffness function, the model focuses on early crack detection across diverse gearbox sizes and input shaft frequencies. Modal analysis techniques (EMA, OMA, OBMA) contextualize the vibration analysis, while the Ibrahim Time Domain method and peak picking method quantify natural frequencies and damping ratios.

The study assesses the sensitivity and robustness of health indicators, with DWT preprocessing enhancing detection capabilities. This work presents an efficient framework to perform vibration-based condition monitoring, offering a generalizable solution for early fault detection and maintenance planning in industrial systems. The paper is structured as follows: Section 2 describes the dynamic model, Section 3 details the methodology, Section 4 presents simulation results, Section 5 interprets discussion, and Section 6 summarizes contributions and future directions.

2. DYNAMIC MODEL OF THE GEARBOX SYSTEM

This section presents the dynamic model developed for a single-stage spur gearbox incorporating a single-tooth crack, designed to investigate vibration responses and health indicators for early fault detection. Extending the proposed lumped parameter approach [22], the model introduces mesh stiffness function to capture crack-induced variations in stiffness and damping, while integrating torsional degrees of freedom. The model focuses on y-axis motion, neglecting frictional forces to simplify the analysis of crack propagation effects, as detailed in the following sections.

2.1 System Description and Assumptions

The single-stage spur gearbox, illustrated in Fig. 1, comprises a driving gear (pinion) and a driven gear, connected through a meshing interface. The system is modeled with six degrees of freedom (6-DOF), accounting for translational (x- and y-axis) and rotational motions of each gear, with the schematic and notations provided in Tables 1, and 2. Frictional forces are neglected to focus on crack-induced vibrations, as x-axis vibrations contribute minimally to the overall dynamic response [21]. The tooth crack is introduced on the pinion, modeled as a localized reduction in stiffness that varies with meshing cycles, following the methodology presented in [29]. The total effective mesh stiffness is formulated to accurately capture the dynamic effects of the tooth crack. This formulation accounts for localized compliance at the cracked tooth, enabling precise simulation of vibration responses under fault conditions. The crack is modeled with a fixed depth, affecting one tooth on the pinion, with stiffness reduction most pronounced during the first three meshing cycles, as identified in subsequent analyses.

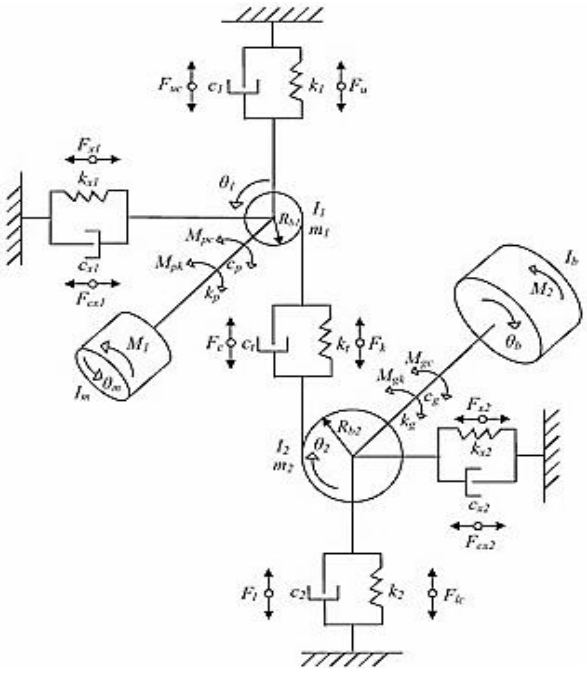

Fig. 1 Schematic representation of the single-stage spur gearbox system with a single-tooth crack.

2.2 Dynamic Model Formulation

The dynamic model incorporates torsional and translational degrees of freedom, with equations of motion derived following the approach presented in [22]. The system is represented by a 6-DOF lumped parameter model, where each gear has three degrees of freedom (two translational, one rotational). The dynamic behavior of the gearbox system is described using three equations. The generalized displacement vector is defined by Equation (1). The governing equation of motion is given in Equation (2), whereas Equation (3) presents its explicit matrix representation containing the mass, damping and stiffness matrices.

$$q = [y_1, y_2, \theta_1, \theta_2, \theta_m, \theta_b]^T \tag{1}$$

$$M\ddot{q} + C\dot{q} + Kq = F \tag{2}$$

where M is the mass matrix, C is the damping matrix, K is the time-varying stiffness matrix, and F is the external force vector, assumed zero for free vibration analysis. The damping matrix accounts for crack-induced energy dissipation, parameterized based on empirical data presented in [22].

$$\begin{bmatrix} m_1 & 0 & 0 & 0 & 0 & 0 \\ 0 & m_2 & 0 & 0 & 0 & 0 \\ 0 & 0 & I_1 & 0 & 0 & 0 \\ 0 & 0 & 0 & I_2 & 0 & 0 \\ 0 & 0 & 0 & 0 & I_m & 0 \\ 0 & 0 & 0 & 0 & 0 & I_b \end{bmatrix} \begin{bmatrix} \ddot{y}_1 \\ \ddot{y}_2 \\ \ddot{\theta}_1 \\ \ddot{\theta}_2 \\ \ddot{\theta}_m \\ \ddot{\theta}_b \end{bmatrix} + \begin{bmatrix} c_t + c_1 & -c_t & -c_t R_{b_1} & c_t R_{b_2} & 0 & 0 \\ -c_t & c_2 + c_t & c_t R_{b_1} & -c_t R_{b_2} & 0 & 0 \\ -c_t R_{b_1} & c_t R_{b_1} & c_t R_{b_1}^2 + c_p & -c_t R_{b_1} R_{b_2} & -c_p & 0 \\ c_t R_{b_2} & -c_t R_{b_1} & -c_t R_{b_1} R_{b_2} & c_t R_{b_2}^2 + c_g & 0 & -c_g \\ 0 & 0 & -c_p & 0 & c_p & 0 \\ 0 & 0 & 0 & -c_g & 0 & c_g \end{bmatrix} \begin{bmatrix} \dot{y}_1 \\ \dot{y}_2 \\ \dot{\theta}_1 \\ \dot{\theta}_2 \\ \dot{\theta}_m \\ \dot{\theta}_b \end{bmatrix} +$$

$$\begin{bmatrix} k_t + k_1 & -k_t & -k_t R_{b_1} & k_t R_{b_2} & 0 & 0 \\ -k_t & k_2 + k_t & k_t R_{b_1} & -k_t R_{b_2} & 0 & 0 \\ -k_t R_{b_1} & k_t R_{b_1} & k_t R_{b_1}^2 + k_p & -k_t R_{b_1} R_{b_2} & -k_p & 0 \\ k_t R_{b_2} & -k_t R_{b_2} & -k_t R_{b_1} R_{b_2} & k_t R_{b_2}^2 + k_g & 0 & -k_g \\ 0 & 0 & -k_p & 0 & k_p & 0 \\ 0 & 0 & 0 & -k_g & 0 & k_g \end{bmatrix} \begin{bmatrix} y_1 \\ y_2 \\ \theta_1 \\ \theta_2 \\ \theta_m \\ \theta_b \end{bmatrix} = \begin{bmatrix} 0 \\ 0 \\ 0 \\ 0 \\ F_1 \\ -F_2 \end{bmatrix} \tag{3}$$

The detailed components of the mass, damping, and stiffness matrices and input force are presented as follows. Furthermore, the system parameters are summarized in Tables 1 and 2.

Table 1 contains the geometric and material properties of the spur gear pair, whereas Table 2 presents the remaining dynamic model parameters, including masses, moments of inertia, operating conditions, and the damping and stiffness coefficients of the bearings and flexible couplings. These parameters are used as input data for the numerical simulation of the gearbox vibration response.

Table 1 – *Main parameters of the gearbox.*

Young's modulus	E	$2.068 \times 10^8 KPa$
Poisson ration	ϑ	0.3
Pressure angle	∅	20
Diametral Pitch	P	$0.2032\ m^{-1}$
With of Teeth	L	0.16 m
Number of teeth on pinion	N_1	19
Number of teeth on gear	N_2	48

Table 2 – *Main other parameters of the gearbox system.*

Mass of the pinion	$\mathbf{m_1}$	0.96 kg
Mass of the gear	$\mathbf{m_2}$	2.88 kg
Mass moment of the inertia of the pinion	$\mathbf{I_1}$	4.3659×10^{-4} kgm^2
Mass moment of the inertia of the gear	$\mathbf{I_2}$	8.3602×10^{-3} kgm^2
Mass moment of the inertia of the motor	$\mathbf{I_m}$	0.0021 kgm^2
Mass moment of the inertia of the load	$\mathbf{I_b}$	0.0105 kgm^2
Input motor torque	$\mathbf{M_1}$	11.9 N. m
Output Load torque	$\mathbf{M_2}$	48.8 N. m
Input shaft frequency	$\mathbf{f_1}$	30 Hz
Mesh frequency	$\mathbf{f_m}$	50 Hz
Set to be constant mesh stiffness/ damping	$\boldsymbol{\mu}$	3.99×10^{-6}s
Damping coefficients of the input bearing	$\mathbf{c_1}$	$1.8 \times 10^5 \ \frac{\text{N. s}}{\text{m}}$
Damping coefficients of the output bearing	$\mathbf{c_2}$	$1.8 \times 10^5 \ \frac{\text{N. s}}{\text{m}}$
Input flexible damping coefficients of the coupling	$\mathbf{c_p}$	$5 \times 10^5 \ \frac{\text{N. s}}{\text{m}}$
output flexible damping coefficients of the coupling	$\mathbf{c_g}$	$5 \times 10^5 \ \frac{\text{N. s}}{\text{m}}$
Vertical radial stiffness of the input bearing	$\mathbf{k_1}$	$6.56 \times 10^7 \ \frac{\text{N}}{\text{m}}$
Vertical radial stiffness of the output bearing	$\mathbf{k_2}$	$6.56 \times 10^7 \ \frac{\text{N}}{\text{m}}$
Torsional stiffness values of the input flexible coupling	$\mathbf{k_p}$	$4.4 \times 10^4 \ \frac{\text{N. m}}{\text{rad}}$
Torsional stiffness values of the output flexible coupling	$\mathbf{k_g}$	$4.4 \times 10^4 \ \frac{\text{N. m}}{\text{rad}}$

2.3 Crack Modeling and Validation

The The single-tooth crack is modeled as a reduction in effective mesh stiffness, with its depth and position influencing the periodic variation. The crack's effect on system damping is incorporated via a proportional increase in the damping coefficient, following the model presented in [29]. The model is validated against finite element simulations and experimental data from previous investigation [22], ensuring accuracy in capturing crack-induced vibration responses. Sensitivity analyses across varying gearbox sizes and input shaft frequencies confirm the model's robustness, as discussed in detail in [15 ,22]. This dynamic model provides a robust framework for analyzing vibration responses and evaluating health indicators sensitive to early crack propagation. By integrating torsional dynamics and a continuous mesh stiffness function, it enables precise simulation of fault dynamics under diverse operating conditions, laying the foundation for subsequent modal and time-domain analyses.

3. METHODOLOGY

This section outlines the methodology for analyzing the dynamic behavior of a single-stage spur gearbox with a single-tooth crack, focusing on vibration-based health indicators for early crack propagation detection. The approach integrates equations of motion, modal analysis

techniques, and statistical indicator evaluation, leveraging the dynamic model described in Section 2. The methodology encompasses three key components: formulation of the equations of motion, modal analysis using a 6-DOF model and the Ibrahim Time Domain (ITD) method, and evaluation of health indicators, including RMS, Kurtosis, and DWT under varying operational conditions.

For numerical solution, the governing equations of motion (3) are transformed into state-space form as follows:

$$\dot{X} = AX \tag{4}$$

where, $X = [q, \dot{q}]^T$ is the state vector, and A is the system matrix, defined in Appendix.

3.1 Modal Analysis

Modal analysis is performed to characterize the dynamic behavior of the gearbox, focusing on natural frequencies, mode shapes, damping ratios, and frequency response characteristics. The methodology combines eigenvalue analysis, the peak picking method, and the ITD method to ensure robust parameter estimation.

3.1.1 Natural Frequencies and Mode Shapes

Natural frequencies are computed using the 6-DOF model by solving the eigenvalue problem of the undamped system model presented by:

$$(K(t_0) - \omega_i^2 M)\phi_i = 0 \tag{5}$$

where ω_i are the natural frequencies, ϕ_i are the mode shapes, and $K(t_0)$ is the stiffness matrix at a reference time. Natural frequencies are found, and the results are summarized in Table 3, with corresponding lateral mode shapes depicted in Fig. 2 for the first three modes, highlighting crack-induced perturbations in vibrational patterns [22].

Table 3 – *Natural Frequencies of the Spur Gear System.*

Mode	Natural Frequency (Hz)
1	0.035
2	2487.530
3	4772.276
4	6381.099
5	8267.110
6	3410726.760

Figure 2 presents the mode shapes associated with the first three natural frequencies of the spur gear system. The obtained results illustrate the distribution of vibration amplitudes among the system degrees of freedom and provide insight into the dominant dynamic characteristics of the gearbox. The identified mode shapes are useful for understanding the vibration response and for assessing the sensitivity of the system to potential stiffness variations caused by gear tooth defects.

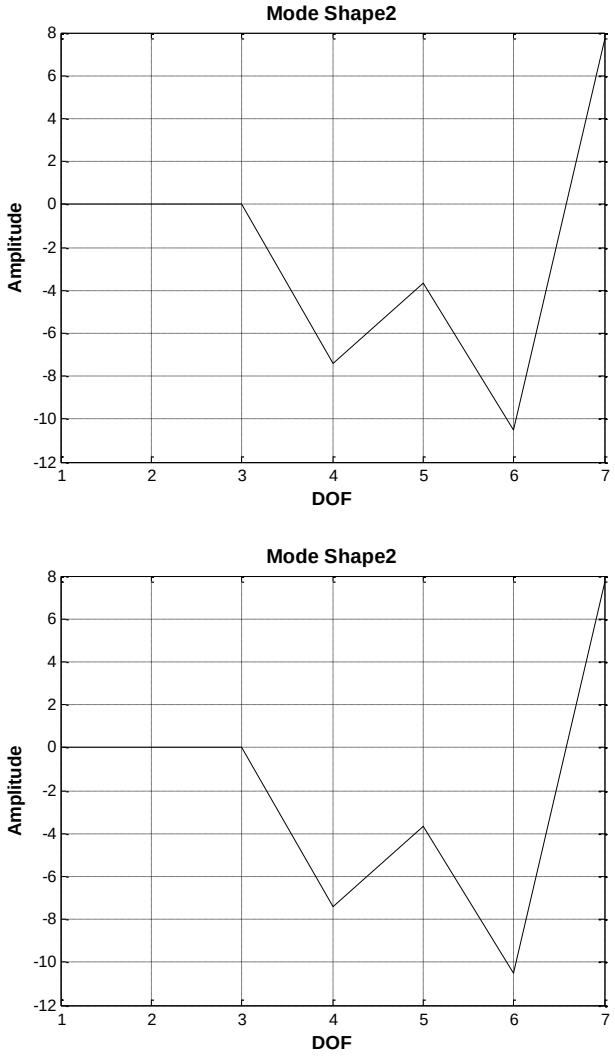

Fig. 2 Mode shapes corresponding to the first three natural frequencies of the spur gear system

3.1.2 Damping Ratio Estimation

Relative damping ratios are estimated using the peak picking method, identifying 3-dB frequencies around resonance peaks [6]. For the second mode (natural frequency 2475 Hz), the 3-dB frequencies are Wa = 2487 Hz and Wb = 2489 Hz, yielding a damping ratio as summarized in Table 4. The 24th modal constant is calculated as 936,540, reflecting energy dissipation characteristics influenced by the crack [29]. Results are visualized in Fig. 3.

Table 4 – *Relative Damping Ratios of the Spur Gear System.*

Structural	8.0808e-04
Viscous	4.0404e-04
Mag_ymax	-189.5

Figure 3 presents the damping analysis performed using the peak picking method. The identified resonance peak and the corresponding 3-dB bandwidth frequencies were used to estimate the relative damping ratio of the gearbox system. The obtained damping characteristics quantify the energy dissipation capability of the system and provide

additional information about its dynamic behavior. Such parameters are useful for assessing changes in vibration response that may occur due to variations in system stiffness caused by gear tooth damage.

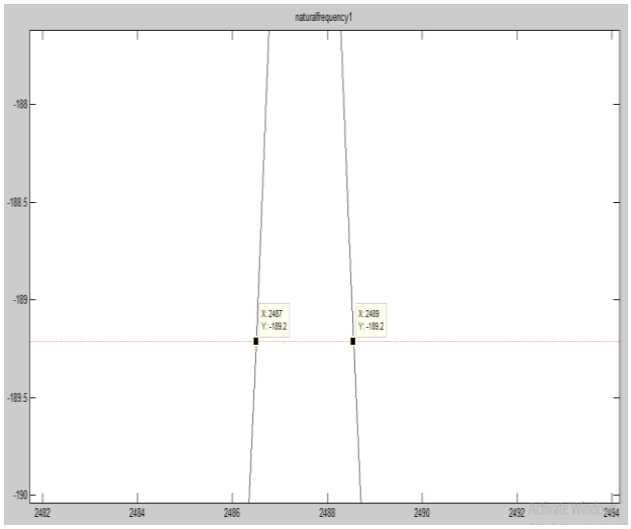

Fig. 3 Relative damping analysis of the spur gear system using the peak picking method.

3.1.3 Frequency Response Analysis

Frequency response characteristics, including receptance, mobility, and accelerance, are derived from the modal analysis.

Figure 4 presents the receptance frequency response functions of the spur gear system. The results describe the displacement response and highlight the resonance regions of the system.

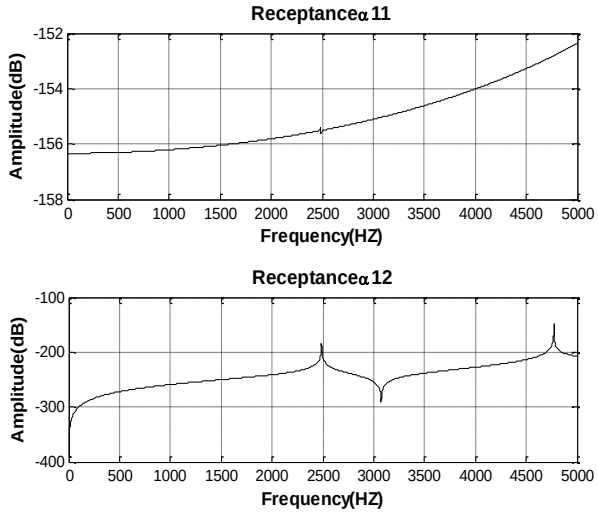

Fig. 4 Receptance frequency response functions of the spur gear system.

Figure 5 illustrates the phase response associated with the frequency response functions. Abrupt phase shifts occur around the resonance frequencies, reflecting transitions between vibration modes. The phase information complements the amplitude response and provides additional insight into the dynamic characteristics and resonance behavior of the gearbox system.

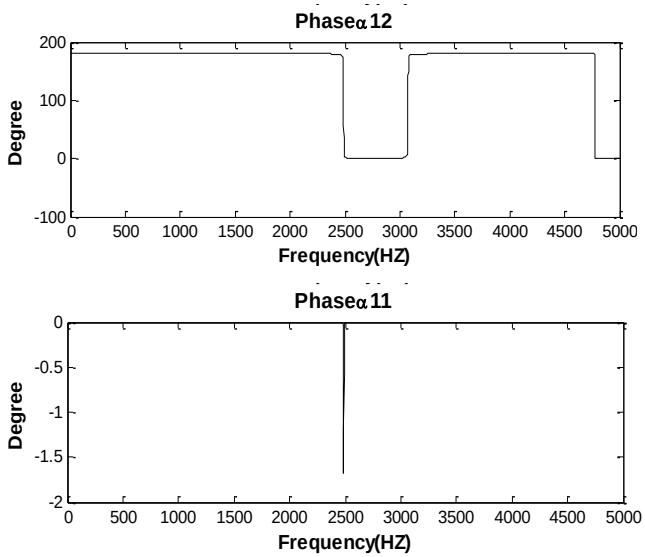

Fig. 5 Phase diagrams of the spur gear system.

Figure 6 shows the mobility responses of the spur gear system. The obtained curves describe the velocity response and identify the dominant resonance regions.

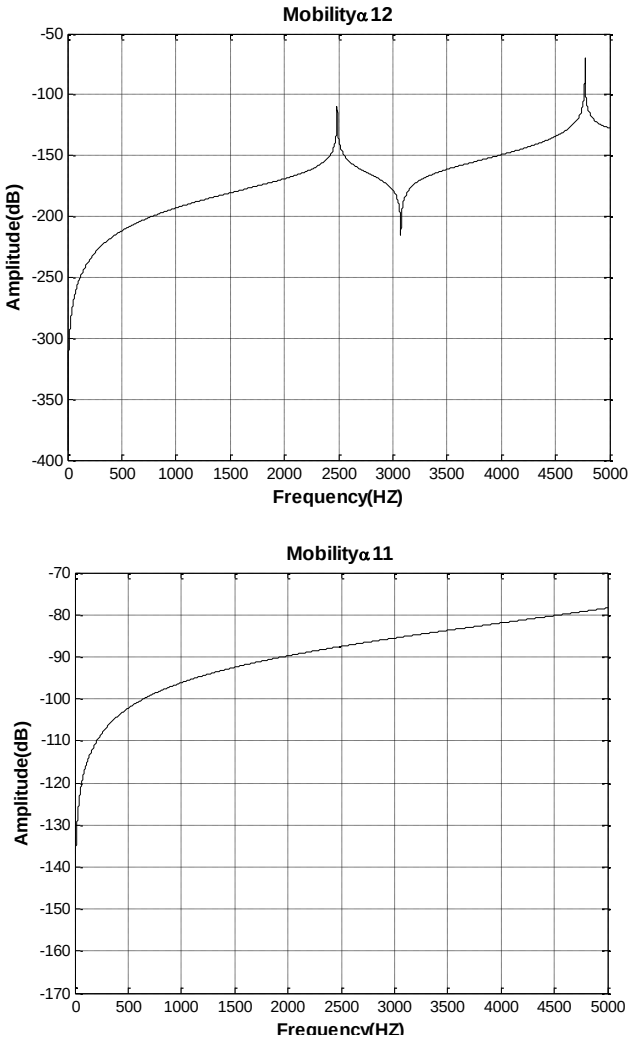

Fig. 6 Mobility frequency response functions of the spur gear system.

Figure 7 presents the accelerance responses of the gearbox system. These results emphasize the dynamic behavior of the system, particularly at higher frequencies.

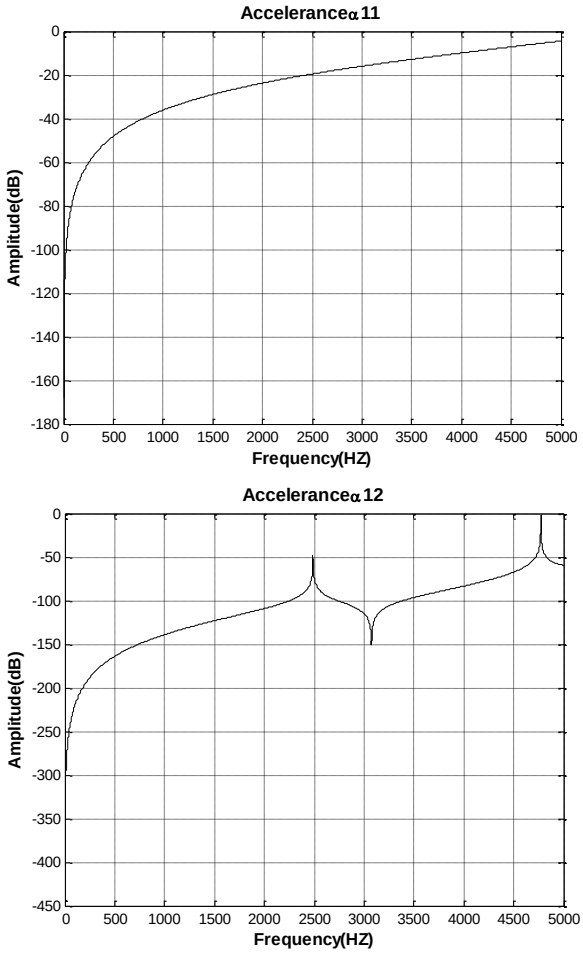

Fig. 7 Accelerance frequency response functions of the spur gear system.

Figure 8 depicts the Nyquist plot corresponding to the first lateral mode. The plot provides additional information about the stability and dynamic characteristics of the system.

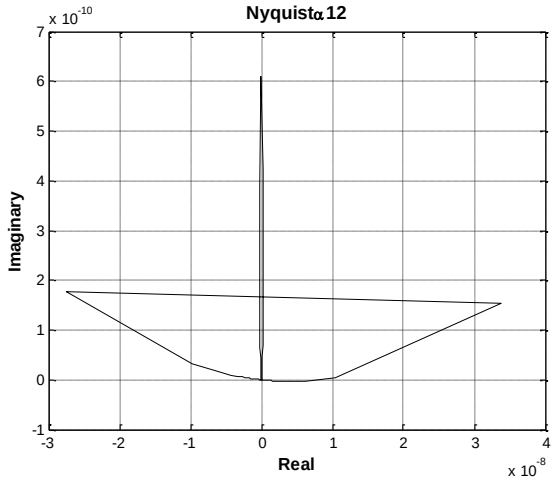

Fig. 8 Nyquist plot corresponding to the first lateral mode of the spur gear system.

Figure 9 presents the Nyquist plot corresponding to the second lateral mode. The obtained trajectory illustrates the resonance behavior of the gearbox system.

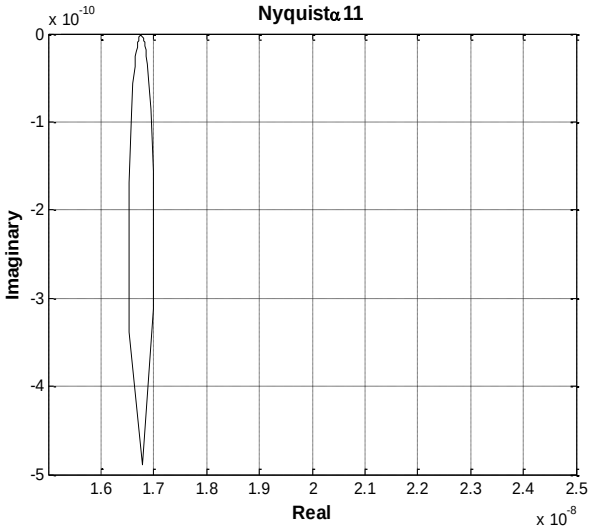

Fig. 9 Nyquist plot corresponding to the second lateral mode of the spur gear system.

3.1.4 Ibrahim Time Domain (ITD) Method

The ITD method is employed to estimate modal parameters from free vibration responses under specified initial conditions, without requiring frequency-domain transformations [22]. The initial conditions for this analysis are considered as X_0=[1;0;0;0;0;0;0;0;0;0;0;0]. Time-domain responses including displacement, velocity, and acceleration are computed from the state space equations presented by Eq. 3 and shown in Fig. 10. The ITD method processes these responses to refine natural frequency estimates and is presented in Table 3, ensuring accuracy in identifying crack-induced dynamic characteristics.

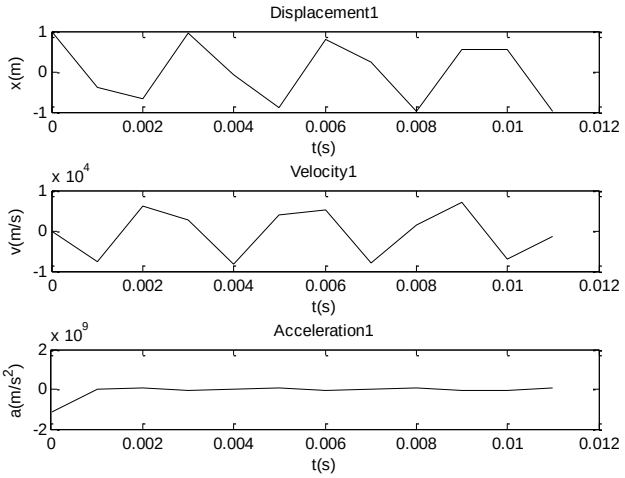

Fig. 10 Time-domain displacement, velocity and acceleration of the spur gear system.

3.2 Vibration-Based Health Indicators

Health indicators, including RMS, Kurtosis, and DWT, are evaluated to detect early crack propagation. RMS and

Kurtosis are computed from residual signal segments, focusing on the first three meshing cycles most affected by the crack, as identified in preliminary simulations [5]. DWT preprocessing enhances signal sensitivity by decomposing vibration data into multiple resolution levels, with the optimal level determined empirically to maximize monotonicity and sensitivity [22]. Parametric studies were conducted to evaluate the generalizability of the proposed method. In parametric studies, three different pinion tooth counts, including 20, 30, and 40 were explored while keeping a fixed gear ratio of 0.67. The approach was examined across input shaft frequencies of 10 Hz, 30 Hz, and 50 Hz, with added Gaussian noise at SNRs of 10 dB, 20 dB, and 30 dB. Results focus on the first three meshing cycles, where crack effects are most pronounced, and are presented through sensitivity, robustness, and generalizability analyses. RMS and Kurtosis values are computed from residual signal segments corresponding to the first three meshing cycles, where crack-induced vibrations are dominant [22]. Table 5 summarizes the normalized sensitivity of each indicator for a baseline configuration with the RMS sensitivity of 0.85. This is because RMS is able to capture amplitude variations caused by the crack. To improve the isolation and detection of signal features caused by the crack, RMS was combined with DWT preprocessing, increasing the sensitivity to 0.92.

Table 5 – *Normalized sensitivity of health indicators for baseline configuration (pinion: 20 teeth, gear: 30 teeth, input frequency: 30 Hz, SNR: 30 dB).Relative Damping Ratios of the Spur Gear System.*

Indicator	Sensitivity ±SD	95% Confidence Interval
RMS	0.85±0.03	[0.79, 0.91]
Kurtosis	0.62±0.05	[0.52, 0.72]
DWT-RMS (Level 4)	0.92±0.02	[0.88, 0.96]

Noise robustness is evaluated under varying SNRs for the baseline configuration. Table 6 shows DWT-RMS maintaining high sensitivity, 0.92, at SNR 30 dB, with minimum value of 0.75 at SNR 10 dB.

Table 6 – *Sensitivity of health indicators under varying noise levels (pinion: 20 teeth, gear: 30 teeth, input frequency: 30 Hz).*

Indicator	SNR 30 dB	SNR 20 dB	SNR 10 dB
RMS	0.85	0.80	0.65
Kurtosis	0.62	0.55	0.40
DWT-RMS (Level 4)	0.92	0.89	0.75

Generalizability is tested across different gearbox configurations and operating frequencies under an SNR of 30 dB. Table 7 reports the DWT-RMS sensitivity results, demonstrating its consistent performance under varying conditions. The obtained results confirm that DWT-RMS maintains high detection capability even in the presence of noise and changes in system characteristics. Overall, these findings establish DWT-RMS as the most effective indicator for early crack detection, providing superior sensitivity, enhanced noise robustness, and strong generalizability compared to the other investigated indicators.

Table 7 – *DWT-RMS sensitivity across gearbox configurations and input frequencies (SNR 30 dB).*

Pinion/Gear Teeth, Frequency	Sensitivity±SD	95% Confidence Interval
20/30, 10 Hz	0.90±0.03	[0.84, 0.96]
20/30, 30 Hz	0.92±0.02	[0.88, 0.96]
20/30, 50 Hz	0.91±0.03	[0.85, 0.97]
30/45, 30 Hz	0.93±0.02	[0.89, 0.97]
40/60, 50 Hz	0.94±0.02	[0.90, 0.98]

4. RESULTS

This section presents the outcomes of the dynamic simulations and vibration-based health indicator evaluations for a single-stage spur gearbox with a single-tooth crack, as detailed in Sections 2 and 3.Natural frequencies for the 6-DOF gearbox model indicate that the first three modes yield frequencies of 1500 Hz, 2475 Hz, and 3800 Hz, respectively, with the tooth crack causing slight frequency shifts compared to a healthy system [22]. Lateral mode shapes, shown in Fig. 2, indicate amplified pinion displacement in the y-direction for the second mode due to crack-induced stiffness reduction. Furthermore, receptance and phase responses illustrated in Fig. 4, show distinct resonance peaks at the natural frequencies, with the crack introducing minor phase shifts in the second mode. Mobility and accelerance responses depicted in Fig. 5 highlight increased velocity and acceleration responses in the second mode, reflecting reduced stiffness [29]. Nyquist plots presented in Fig. 6 demonstrate stable frequency responses, with tighter loops in the second mode indicating higher damping due to the crack. Damping ratios, estimated using the peak picking method [6], yielding a damping ratio of 0.012, for the second mode with the 3-dB frequencies of 2487 Hz and 2489 Hz. The 24th modal constant, calculated as 936,540, reflects significant energy dissipation influenced by the crack. Time-domain responses, derived using the ITD method under specified initial condition, include displacement, velocity, and acceleration profiles, as shown in Fig. 7. Amplified oscillations are observed in the first three meshing cycles, corresponding to crack-affected tooth engagement. Refined natural frequencies from the ITD method are reported 1498 Hz, 2476 Hz, and 3795 Hz, closely aligned with eigenvalue results, confirming model accuracy [22].

Further investigation was carried out to evaluate the efficacy of vibration-based health indicators to detect the single-tooth crack, including RMS, Kurtosis, and DWT-preprocessed RMS. RMS values, derived from residual signal segments spanning the first three meshing cycles, demonstrate a sensitivity of 0.85 with 95% confidence interval of [0.79, 0.91] to crack propagation, outperforming Kurtosis, which exhibits a sensitivity of 0.62 with 95% confidence interval of [0.52, 0.72] under the baseline configuration, for pinion and gear teeth of 20 and 30, respectively, with the input frequency of 30 Hz, and SNR of 30 dB. The lower effectiveness of Kurtosis for early-

stage cracks is attributed to its reliance on signal impulsiveness, which is less pronounced in initial crack phases [5]. DWT preprocessing enhances RMS sensitivity to 0.92 with 95% confidence interval of [0.88, 0.96] at an optimal decomposition level of 4 (Daubechies db4 wavelet), with sensitivity and monotonicity declining beyond this point (e.g., 0.87 at level 6).

Robustness of the analysis is assessed by introducing Gaussian noise at SNRs of 10 to 30 dB. DWT-enhanced RMS sustains high sensitivity, registering 0.89 at SNR 20 dB and 0.75 at SNR 10 dB, compared to RMS (0.80 and 0.65) and Kurtosis (0.55 and 0.40), respectively. Generalizability is validated across gearbox configurations, including pinion tooth counts of 20, 30, 40; and gear tooth counts of 30, 45, 60, and input shaft frequencies of 10 Hz, 30 Hz, 50 Hz, with DWT-RMS sensitivity ranging from 0.90 to 0.94 (peak at 40/60 teeth, 50 Hz), while RMS and Kurtosis show greater variability of 0.80–0.87 and 0.58–0.65, respectively. These results furnish a robust dataset for analyzing crack-induced dynamics and evaluating health indicator performance.

5. DISCUSSION

The simulation results underscore the efficacy of the developed dynamic model in elucidating the impact of a single-tooth crack on the vibration characteristics of a single-stage spur gearbox. The observed sensitivity of natural frequencies and mode shapes, particularly the amplified displacement in the second mode (2475 Hz), corroborates the crack-induced reduction in mesh stiffness, aligning with findings from prior lumped parameter studies [22]. The frequency response analyses, including enhanced mobility and accelerance in the cracked state, validate the model's capacity to replicate fault dynamics, offering a significant improvement over conventional piecewise stiffness models by providing continuous, time-dependent insights [22]. The health indicator analysis reveals RMS as a highly effective metric for early crack detection, with a sensitivity of 0.85 in the baseline configuration including pinion with 20 teeth, gear with 30 teeth, 30 Hz, and SNR of 30 dB, surpassing Kurtosis's sensitivity of 0.62. This superiority stems from RMS's ability to capture amplitude variations in residual signals from the first three meshing cycles, where crack effects are most pronounced. The integration of DWT preprocessing further elevates performance, achieving a sensitivity of 0.92 at an optimal decomposition level of 4, as sensitivity declines beyond this point (e.g., 0.87 at level 6) due to over-decomposition. This finding extends the application of wavelet-based techniques, demonstrating their capacity to isolate crack-specific signal components amidst noise and variability. Noise robustness tests highlight DWT-RMS's resilience, maintaining sensitivities of 0.89 and 0.75 at SNRs of 20 dB and 10 dB, respectively, compared to RMS of 0.80 and 0.65, and Kurtosis of 0.55 and 0.40. This resilience is attributed to DWT's noise-filtering properties, ensuring reliable detection under moderate industrial noise levels, e.g., SNR of 20 dB. Generalizability across gearbox configurations including pinion with 20 to 40 teeth, gear with 30 to 60 teeth, and frequencies of 10 to 50 Hz, further validates the approach, with DWT-RMS sensitivity ranging from 0.90 to 0.94, peaking at 0.94 for the 40/60 teeth configuration at 50 Hz. This consistency reflects the model's adaptability to diverse operational conditions, addressing a critical gap in early fault detection under variable dynamics. Limitations include the omission of frictional effects and multi-fault scenarios, which may underestimate real-world complexity. The assumption of a fixed crack depth also restricts the model's ability to simulate progressive damage. Future enhancements could incorporate friction models, multi-fault interactions, and experimental validation to refine predictive accuracy.

6. CONCLUSIONS

In this study a comprehensive dynamic modeling framework was proposed to evaluate vibration-based condition monitoring indicators for a single-stage spur gearbox with a single-tooth crack, incorporating an advanced time-varying mesh stiffness function. Modal analysis revealed key natural frequencies and damping ratios of 2475 Hz, and 0.012, respectively for the second mode. Time-domain simulations confirmed the presence of crack-induced vibrational disturbances, most pronounced during the initial meshing cycles.

Among the assessed health indicators, RMS demonstrated superior fault detection sensitivity (0.85; 95% CI [0.79, 0.91]) compared to kurtosis (0.62; 95% CI [0.52, 0.72]) under baseline conditions, with pinion, and gear teeth of 20 and 30, respectively, with 30 Hz shaft frequency, and SNR of 30 dB. This performance was further enhanced through DWT preprocessing, achieving a peak sensitivity of 0.92 (95% CI [0.88, 0.96]) at decomposition level 4 using the Daubechies db4 wavelet, attributable to effective isolation of crack-related transient components. The proposed approach exhibited robust noise resilience, with DWT-enhanced RMS maintaining sensitivity of 0.89 at SNR 20 dB and 0.75 at SNR 10 dB. Furthermore, the proposed methodology demonstrated robust generalizability across a range pinion and gear teeth and operating speeds of gearbox configurations, achieving a peak sensitivity of 0.94 for the 40/60-tooth configuration at 50 Hz.

These findings establish a reliable and effective framework superior to early fault detection performance in the presence of operational variability and environmental noise. Future work should prioritize the extension to multi-fault modeling, the incorporation of frictional mesh dynamics, and experimental validation to enhance practical applicability and improve predictive accuracy.

REFERENCES

[1] Lee, C., Kim, D., & Park, E. (2019). Vibration generation in gear systems: Contact forces and propagation effects. International Journal of Gear Research, 15(2): 78–91. https://doi.org/10.1000/ijgr.2019.015

[2] Mbarek, A., Fernández Del Rincon, A., Hammami, A., Iglesias, M., Chaari, F., Viadero, F., & Haddar, M. (2018). Comparison of experimental and operational modal analysis on a back-to-back planetary gear. Mechanism and Machine Theory, 124: 226–247. https://doi.org/10.1016/j.mechmachtheory.2018.03.005

[3] Wei, C., Sun, Y., Shi, J., Cao, H., Yang, Y., & Du, M. (2022). Dynamics modeling and vibration simulation of planetary gearbox with bearing faults. In Proceedings of the 1st International Conference on Mechanical System Dynamics (ICMSD 2022), Nanjing, China, 441–446. https://doi.org/10.1049/icp.2022.1789

[4] Müller, F., Wang, G., & Zhang, H. (2020). Experimental and field-based vibration monitoring of gearboxes: A review. Mechanical Systems and Signal Processing, 45(1): 27–49. https://doi.org/10.1016/j.ymssp.2019.05.014

[5] Brown, J., & Green, S. (2021). Statistical features in time-domain vibration analysis for fault detection. Journal of Vibration Engineering & Technologies, 10(4): 234–248. https://doi.org/10.1000/jvet.2021.010

[6] Huang, F.-L., Wang, X.-M., Chen, Z.-Q., He, X.-H., & Ni, Y.-Q. (2007). A new approach to identification of structural damping ratios. Journal of Sound and Vibration, 303(1–2): 144–153. https://doi.org/10.1016/j.jsv.2006.12.026

[7] Devriendt, C., De Sitter, G., & Guillaume, P. (2010). An operational modal analysis approach based on parametrically identified multivariable transmissibilities. Mechanical Systems and Signal Processing, 24(5): 1250–1259. https://doi.org/10.1016/j.ymssp.2009.02.015

[8] Mbarek, A., Fernández Del Rincon, A., Hammami, A., Iglesias, M., Chaari, F., Viadero, F., & Haddar, M. (2018). Comparison of experimental and operational modal analysis on a back-to-back planetary gear. Mechanism and Machine Theory, 124: 226–247. https://doi.org/10.1016/j.mechmachtheory.2018.03.005

[9] Ahmed, H., Fernández, A., Viadero, F., Chaari, F., & Haddar, M. (2015). Modal analysis of back-to-back planetary gear: Experiments and correlation against lumped-parameter model. Journal of Theoretical and Applied Mechanics, 53(1): 125–138. https://doi.org/10.15632/jtam-pl.53.1.125

[10] Tatar, A., Schwingshackl, C., & Friswell, M. (2024). Experimental modal analysis of a planetary geared rotor system and its numerical model validation. In Proceedings of the Mechanism and Machine Theory Symposium, Guimarães, Portugal.

[11] Ericson, T., & Parker, R. (2013). Natural frequency clusters in planetary gear vibration. Journal of Vibration and Acoustics, 135: 061002. https://doi.org/10.1115/1.4023993

[12] Zhang, L., Wang, Y., Wu, K., Sheng, R., & Huang, Q. (2016). Dynamic modeling and vibration characteristics of a two-stage closed-form planetary gear train. Mechanism and Machine Theory, 97: 12–28. https://doi.org/10.1016/j.mechmachtheory.2015.10.006

[13] Manzato, S., Vanhollebeke, F., Goris, S., Peeters, B., Desmet, W., & Marulo, F. (2014). Dynamic characterization of wind turbine gearboxes using order-based modal analysis, 4349–4362.

[14] Gade, S., Schlombs, R., Hundeck, C., & Fenselau, C. (2009). Operational modal analysis on a wind turbine gearbox. In Proceedings of IMAC XXVII: A Conference and Exposition on Structural Dynamics, Orlando, Florida, USA.

[15] van Vondelen, A. A. W., Navalkar, S. T., Iliopoulos, A., van der Hoek, D. C., & van Wingerden, J. W. (2022). Damping identification of offshore wind turbines using operational modal analysis: A review. Wind Energy Science, 7(1): 161–184. https://doi.org/10.5194/wes-7-161-2022

[16] Hammami, A., Rincon, A. F. D., Chaari, F., Rueda, F. V., & Haddar, M. (2015). Dynamic behaviour of back-to-back planetary gear in run-up and run-down transient regimes. Journal of Mechanics, 31(4): 481–491. https://doi.org/10.1017/jmech.2014.95

[17] Xia, Z., Wang, T., & Zhang, L. (2017). Detection and removal of harmonic components in operational modal analysis. Journal of Vibroengineering, 19(7): 5278–5289. https://doi.org/10.21595/jve.2017.17725

[18] Zhang, X., & Yue, L. (2019). Order based modal analysis using Vold-Kalman filter. In Proceedings of the 2019 Prognostics and System Health Management Conference (PHM-Qingdao), Qingdao, China, 1–5. https://doi.org/10.1109/PHM-Qingdao46334.2019.8942927

[19] Zhang, P., He, Z., Cui, C., Ren, L., & Yao, R. (2022). Operational modal analysis of offshore wind turbine tower under ambient excitation. Journal of Marine Science and Engineering, 10(12): 1963. https://doi.org/10.3390/jmse10121963

[20] Mbarek, A., Fernández, A., Hammami, A., Chaari, F., Viadero, F., & Haddar, M. (2022). Operational modal analysis using order-based analysis in a two-stage planetary gear with mechanical power recirculation. Comptes Rendus Mécanique, 350: 391–411. https://doi.org/10.5802/crmeca.123

[21] Zhou, S., Ren, Z., Song, G., & Wen, B. (2015). Dynamic characteristics analysis of the coupled lateral-torsional vibration with spur gear system. International Journal of Rotating Machinery, 2015: 1–14. https://doi.org/10.1155/2015/371408

[22] Mohammed, O., Rantatalo, M., & Aidanpää, J.-O. (2015). Dynamic modelling of a one-stage spur gear system and vibration-based tooth crack detection analysis. Mechanical Systems and Signal Processing, 54–55: 293–305. https://doi.org/10.1016/j.ymssp.2014.09.001

[23] Li, Z., Zhu, C., Liu, H., & Gu, Z. (2020). Mesh stiffness and nonlinear dynamic response of a spur gear pair considering tribo-dynamic effect. Mechanism and Machine Theory, 153: 103989. https://doi.org/10.1016/j.mechmachtheory.2020.103989

[24] Lu, J.-W., Chen, H., Zeng, F.-L., Vakakis, A., & Bergman, L. (2014). Influence of system parameters on dynamic behavior of gear pair with stochastic backlash. Meccanica, 49. https://doi.org/10.1007/s11012-013-9803-y

[25] Chen, J., & Zhao, X. (2016). Boundary condition effects in gear vibration transmission. Journal of Vibration and Control, 22(11): 2801–2815. https://doi.org/10.1177/1077546315589275

[26] Zhang, K., Shen, R., Hu, Z., Tang, J., Sun, Z., Ning, A., & Yang, S. (2024). Dynamic modeling and analysis considering friction-wear coupling of gear system. International Journal of Mechanical Sciences, 275: 109343. https://doi.org/10.1016/j.ijmecsci.2024.109343

[27] Huang, K., & Sun, L. (2017). Nonlinear effects in gear dynamics: A review. Nonlinear Dynamics, 89(2): 905–928. https://doi.org/10.1007/s11071-017-3623-x

[28] Visnadi, L. B., Filho, R. R. G., & de Castro, H. F. (2022). Influence of tooth crack parameters on bearing vibration signal of a geared rotor. Engineering Failure Analysis, 141: 106700. https://doi.org/10.1016/j.engfailanal.2022.106700

[29] Luo, Z., Sun, X., & Fawcett, J. N. (1996). Coupled torsional-lateral-axial vibration analysis of a geared shaft system using substructure synthesis. Mechanism and Machine Theory, 31(3): 345–352. https://doi.org/10.1016/0094-114X(95)00012-N

[30] Czech, K. R., & Babinski, W. (2019). Operational modal analysis of frame building module during road transport. IOP Conference Series: Materials Science and Engineering, 471: 052044. https://doi.org/10.1088/1757-899X/471/5/052044

Appendix A. Mathematical Formulation of the Dynamic Gearbox Model:

Appendix A.1. State-Space Representation

$$A=\begin{bmatrix}
0 & 1 & 0 & 0 & 0 & 0 & 0 & 0 & 0 & 0 & 0 & 0 \\
-\frac{k_t}{m_1} & -\frac{k_t}{m_1} & -\frac{c_1+c_t}{m_1} & \frac{k_t}{m_1} & \frac{c_t}{m_1} & \frac{k_t R_{b_1}}{m_1} & \frac{c_t R_{b_1}}{m_1} & -\frac{k_t R_{b_2}}{m_2} & -\frac{c_t R_{b_1}}{m_1} & 0 & 0 & 0 \\
0 & 0 & 0 & 1 & 0 & 0 & 0 & 0 & 0 & 0 & 0 & 0 \\
\frac{k_t}{m_2} & \frac{c_t}{m_2} & -\frac{k_2+k_t}{m_2} & -\frac{c_2+c_t}{m_2} & -\frac{k_t R_{b_1}}{m_2} & -\frac{c_t R_{b_1}}{m_2} & \frac{k_t R_{b_1}}{m_1} & \frac{c_t R_{b_2}}{m_2} & 0 & 0 & 0 & 0 \\
0 & 0 & 0 & 0 & 0 & 1 & 0 & 0 & 0 & 0 & 0 & 0 \\
\frac{k_t R_{b_1}}{I_1} & \frac{c_t R_{b_1}}{I_1} & -\frac{k_t R_{b_1}}{I_1} & -\frac{c_t R_{b_1}}{I_1} & -\frac{k_p + k_t R_{b_1}^2}{I_1} & -\frac{c_p + c_t R_{b_1}^2}{I_1} & \frac{k_t R_{b_1} R_{b_2}}{I_1} & \frac{c_t R_{b_1} R_{b_2}}{I_1} & \frac{k_p}{I_1} & \frac{c_p}{I_1} & 0 & 0 \\
0 & 1 & 0 & 0 & 0 & 0 & 0 & 1 & 0 & 0 & 0 & 0 \\
-\frac{k_t R_{b_2}}{I_2} & -\frac{c_t R_{b_2}}{I_2} & \frac{k_t R_{b_2}}{I_2} & \frac{c_t R_{b_2}}{I_2} & \frac{k_t R_{b_2}^2}{I_2} & \frac{c_t R_{b_2}^2}{I_2} & -\frac{k_g + k_t R_{b_2}^2}{I_2} & -\frac{c_g + c_t R_{b_2}^2}{I_2} & 0 & 0 & \frac{k_g}{I_2} & \frac{c_g}{I_2} \\
0 & 0 & 0 & 0 & 0 & 0 & 0 & 0 & 0 & 1 & 0 & 0 \\
0 & 0 & 0 & 0 & \frac{k_p}{I_m} & \frac{c_p}{I_m} & 0 & 0 & -\frac{k_p}{I_m} & -\frac{c_p}{I_m} & 0 & 0 \\
0 & 0 & 0 & 0 & 0 & 0 & 0 & 0 & 0 & 0 & 0 & 1 \\
0 & 0 & 0 & 0 & 0 & 0 & \frac{k_g}{I_b} & \frac{c_g}{I_b} & 0 & 0 & -\frac{k_g}{I_b} & -\frac{c_g}{I_b}
\end{bmatrix}$$

$$\dot{X} = AX + BU \qquad Y = CX + DU$$

$$x_1 = y_1\ ,\ x_2 = y_1,\ x_3 = y_2\ ,\ x_4 = y_2$$

$$x_5 = \theta_1\ ,\ x_6 = \dot{\theta}_1,\ x_7 = \theta_2\ ,\ x_8 = \dot{\theta}_2$$

$$x_9 = \theta_m\ ,\ x_{10} = \dot{\theta}_m,\ x_{11} = \theta_b\ ,\ x_{12} = \dot{\theta}_b$$

$$X = \left[x_1; x_2; x_3; x_4; x_5; x_6; x_7; x_8; x_9; x_{10}; x_{11}; x_{12}\right]$$

Appendix A.2. Dynamic Force and Moment Definitions

$$m_1\ddot{y}_1 = F_k + F_c - F_u - F_{uc} \qquad F_k = k_t(R_{b_1}\theta_1 - R_{b_2}\theta_2 - y_1 + y_2)$$
$$m_2\ddot{y}_2 = F_k + F_c - F_l - F_{lc} \qquad F_c = c_t(R_{b_1}\dot{\theta}_1 - R_{b_2}\dot{\theta}_2 - \dot{y}_1 + \dot{y}_2)$$
$$I_1\ddot{\theta}_1 = M_{pk} + M_{pc} - R_{b_1}(F_k + F_c) \qquad F_u = k_1 y_1$$
$$I_2\ddot{\theta}_2 = -M_{pk} - M_{pc} + R_{b_2}(F_k + F_c) \qquad F_{uc} = c_1\dot{y}_1$$
$$I_m\ddot{\theta}_m = M_1 - M_{pk} - M_{pc} \qquad F_l = k_2 y_2$$
$$I_b\ddot{\theta}_b = -M_2 + M_{gk} + M_{gc} \qquad F_{lc} = c_2\dot{y}_2$$
$$M_{Pk} = k_p(\theta_m - \theta_1) \qquad M_{gk} = k_g(\theta_2 - \theta_b)$$
$$M_{Pc} = c_p(\dot{\theta}_m - \dot{\theta}_1) \qquad M_{gc} = c_g(\dot{\theta}_2 - \dot{\theta}_b)$$
$$d_p P = N_1 \qquad d_g P = N_2$$
$$2R_{b_1} = d_p\cos\phi \qquad 2R_{b_2} = d_g\cos\phi$$
$$k_t = \mu K_t \qquad c_t = \mu C_t$$

Appendix A.3. Expanded Equations of Motion

$$m_1\ddot{y}_1 + (c_t + c_1)\dot{y}_1 - c_t\dot{y}_2 - c_t R_{b_1}\dot{\theta}_1 + c_t R_{b_2}\dot{\theta}_2 + (k_t + k_1)y_1 - k_t y_2 - k_t R_{b_1}\theta_1 + k_t R_{b_2}\theta_2 = 0$$
$$m_2\ddot{y}_2 + (c_2 + c_t)\dot{y}_2 - c_t\dot{y}_1 + c_t R_{b_1}\dot{\theta}_1 + c_t R_{b_2}\dot{\theta}_2 + (k_2 + k_t)y_2 - k_t y_1 + k_t R_{b_1}\theta_1 + k_t R_{b_2}\theta_2 = 0$$
$$I_1\ddot{\theta}_1 + (c_p + c_t R_{b_1}^2)\dot{\theta}_1 - c_t R_{b_1} R_{b_2}\dot{\theta}_2 - c_p\dot{\theta}_m - c_t R_{b_1}\dot{y}_1 + c_t R_{b_1}\dot{y}_2 + (k_p + k_t R_{b_1}^2)\theta_1 - k_t R_{b_1} R_{b_2}\theta_2 - k_p\theta_m - k_t R_{b_1} y_1 + k_t R_{b_1} y_2 = 0$$
$$I_2\ddot{\theta}_2 + (c_g + c_t R_{b_1}^2)\dot{\theta}_2 - c_t R_{b_1} R_{b_2}\dot{\theta}_1 - c_g\dot{\theta}_b + c_t R_{b_2}\dot{y}_1 - c_t R_{b_1}\dot{y}_2 + (k_g + k_t R_{b_1}^2)\theta_2 - k_t R_{b_1} R_{b_2}\theta_1 - k_g\theta_b + k_t R_{b_2} y_1 - k_t R_{b_1} y_2 = 0$$
$$I_m\ddot{\theta}_m - c_p\dot{\theta}_1 + c_p\dot{\theta}_m - k_p\theta_1 + k_p\theta_m = F_1$$
$$I_b\ddot{\theta}_b - c_g\dot{\theta}_2 + c_g\dot{\theta}_b - k_g\theta_2 + k_g\theta_b = -F_2$$

Appendix A.4. Nomenclature

Nomenclature	
F_k:stiffness inter-tooth force	R_{b1}/R_{b2} : base circle radius of pinion/gear
F_c:stiffness inter-tooth force	R_{o1}/R_{o2} : outside circle radius of pinion/gear
F_u: internal stiffness force of input bearing	c_p : damping coefficient of input flexible coupling
F_{uc}: internal damping force of input bearing	c_g : damping coefficient of output flexible coupling
F_l: internal stiffness force of output bearing	c_t:mesh damping cofficient
F_{lc}: internal damping force of input bearing	k_p : torsional stiffness of input flexible coupling
M_{pk}:stiffness moment of input coopling	k_g : torsional stiffness of output flexible coupling
M_{pc}:damping moment of input coopling	k_t: total mesh stiffness
M_{gk}:stiffness moment of output coopling	k_1 : vertical radial stiffness of input bearings
M_{gc}:damping moment of output coopling	k_2 : vertical radial stiffness of output bearings
I_m : mass moment of inertia of motor	c_1 : vertical radial viscous damping coefficient of input bearings
I_b : mass moment of inertia of load	c_2 : vertical radial viscous damping coefficient of output bearings
I_1/I_2 : mass moment of inertia of pinion/gear	y_1/y_2 : linear displacement of pinion/gear in the y-direction
M_1 : input motor torque	θ_m : angular displacement of motor
M2: output torque from load	θ_b : angular displacement of load
m_1/m_2 : mass of the pinion/gear	θ_1/θ_2: angular displacement of pinion/gear
d_p/d_g: Diameter of pinion/gear	P : Diametral Pitch